Journal of the European Ceramic Society xxx (xxxx) xxx

Contents lists available at ScienceDirect

Journal of the European Ceramic Society

journal homepage: www.elsevier.com/locate/jeurceramsoc

Microwave dielectric properties of a low firing and temperature stable lithium magnesium tungstate (Li_4MgWO_6) ceramic with a rock-salt variant structure

Xing Zhang [a,b,d], Zixuan Fang [a,b,c,*], Yinghao Jiang [a,b], Mingxia Wang [a,b], Stephen Gee [e], Lei Zhou [f], Hongyu Yang [a,b], Feng Si [a,b], Peng Zhao [a,b], Zhe Xiong [a,b], Shuren Zhang [a,b], Bin Tang [a,b,**]

[a] State Key Laboratory of Electronic Thin Films and Integrated Devices, University of Electronic Science and Technology of China, Chengdu 611731, China
[b] National Engineering Research Center of Electromagnetic Radiation Control Materials, University of Electronic Science and Technology of China, Chengdu 611731, China
[c] School of Materials and Energy, University of Electronic Science and Technology of China, Chengdu 611731, China
[d] Department of Mechanical Engineering, National University of Singapore, 117575, Singapore
[e] Department of Materials Science and Engineering, University of California Berkeley, Berkeley, CA 94720, United States
[f] School of Communication and Information Engineering, Chongqing University of Posts and Telecommunications, Chongqing 400065, China

ARTICLE INFO

Keywords:
Li_4MgWO_6
LTCC
Temperature stable
Rock salt

ABSTRACT

The Li_4MgWO_6 ceramic was synthesized by the conventional solid-state reaction method, and its sintering behavior and microwave dielectric properties were studied for the first time. The XRD patterns and structural refinements indicated that Li_4MgWO_6 formed an orthorhombic phase at temperatures above 900 °C, and TEM analyses confirmed the ordered and layered rock-salt superstructures for the orthorhombic Li_4MgWO_6. The SEM photographs and relative density curve showed that the sample sintered at 950 °C had the highest densification. When sintered at 950 °C in a WO_3-rich atmosphere for 4 h, Li_4MgWO_6 had the following optimum properties: ε_r = 15.06±0.33, $Q\times f$ = 28,300±600 GHz (f = 10.1 GHz), and τ_f = 0.9±3.4 ppm/°C. Compared with other reported low permittivity compounds, Li_4MgWO_6 shows more potential for the Low-Temperature Cofired Ceramics (LTCC) substrate materials due to its intrinsic low sintering temperature, novel temperature stability, and relatively low dielectric loss.

1. Introduction

Low dielectric permittivity plays a vital role in the propagation of high-velocity signals through a dielectric medium, and dielectric materials with low permittivities (ε_r, generally less than 20) are frequently used as substrate materials for millimeter-wave applications [1–3]. The low-temperature co-fired ceramic (LTCC) technology is one of the most important methods for integrating chip components on dielectric substrates [4]. The materials for LTCC applications should have sintering temperatures lower than the melting point of the co-fired electrodes, of which the most commonly used electrode is silver with a melting point of 961 °C. Unfortunately, numerous promising substrate candidates, such as Mg_2SiO_4 (1450 °C) [5], $ZnAl_2O_4$ (1375 °C) [6], $CaMgSi_2O_6$ (1300 °C) [7], $Li_3Mg_2NbO_6$ (1250 °C) [8], Li_2TiO_3 (1230 °C) [9], and Li_3NbO_4 (1150 °C) [8] possess relatively high sintering temperatures. Recent efforts have focused on modifying the dielectric properties of rock-salt structured $Li_3Mg_2NbO_6$, Li_2TiO_3, and Li_3NbO_4-based ceramics for LTCC applications as these lithium-containing ceramics have lower sintering temperatures near the LTCC requirement [10–12]. In these ceramics, stability over a wide range of temperatures is vital for practical applications of LTCC materials, but most of the low permittivity matrix ceramics possess negative temperature coefficients of the resonant frequency (τ_f) [13]; only a few exhibited positive τ_f values, such as Li_2SnO_3 (ε_r = 12.8, $Q \times f$ = 20,800 GHz, τ_f = 26.9 ppm/°C) [9], Li_2TiO_3 (ε_r =

* Corresponding author at: School of Materials and Energy, University of Electronic Science and Technology of China, Chengdu 611731, China.
** Corresponding author at: State Key Laboratory of Electronic Thin Films and Integrated Devices, University of Electronic Science and Technology of China, Chengdu 611731, China.
E-mail addresses: zixuanfang@uestc.edu.cn (Z. Fang), tangbin@uestc.edu.cn (B. Tang).

https://doi.org/10.1016/j.jeurceramsoc.2021.09.010
Received 10 April 2021; Received in revised form 23 August 2021; Accepted 5 September 2021
Available online 10 September 2021

19.8, $Q \times f$ = 23,600 GHz, τ_f = 38.5 ppm/°C) [9], $NiCu_2Nb_2O_8$ (ε_r = 12.8, $Q \times f$ = 4200 GHz, τ_f = 481.6 ppm/°C) [14], and $LaNbO_4$ (ε_r = 19.3, $Q \times f$ = 54,400 GHz, τ_f = 9.0 ppm/°C) [15], and it is rare that a low-permittivity compound has a near-zero τ_f value. While a near-zero τ_f can be achieved by compositing two phases with opposite τ_f values, other properties would be influenced. Similarly, while the sintering temperature could be reduced by introducing a glassy phase into the ceramic material, such a change would likely alter the dielectric permittivity and thermal stability as well as deteriorate the $Q \times f$ values [16]. Therefore, it would be complex to develop a new glass-ceramic composite to satisfy the needs of LTCC applications. It frequently requires trial-and-error tests to find both an appropriate glass additive and a dopant phase with an opposite τ_f to the matrix to modify both the sintering temperature and temperature stability in the meantime. However, luckily, glass-free ceramics with intrinsically low sintering temperatures were more beneficial for performance modification, saving time and cost for the formula research and production of complex glass additives. Numerous recently developed glass-free ceramics concerning Bi, Mo, V, and W-based compounds, are well-suited for LTCC applications [17–19].

Specifically, lithium tungsten oxide glass-free microwave dielectric ceramics have received much attention due to their excellent dielectric performance. For example, Li_4WO_5 has a pure rock-salt phase and novel temperature-stable properties as ε_r = 8.6, $Q \times f$ = 23,100 GHz, and τ_f = -2.6 ppm/°C when sintered at 890 °C for 2 h [20]. The phenacite Li_2WO_4 ceramic has a quite low intrinsic sintering temperature, and it showed good properties of ε_r = 5.5, $Q \times f$ = 62,000 GHz, and τ_f = -146 ppm/°C when sintered at 650 °C for 2 h [21]. Also, the lithium magnesium tungstate ceramics, chemically formulated as $Li_2Mg_2W_2O_9$ and $Li_2Mg_2(WO_4)_3$, showed good dielectric performance. The former showed the properties of ε_r = 11.5, $Q \times f$ = 31,900 GHz, and τ_f = -66 ppm/°C when well-sintered at 920 °C for 4 h, and the latter showed the properties of ε_r = 8.2, $Q \times f$ = 90,000 GHz, and τ_f = -52.4 ppm/°C when sintered at 900 °C for 4 h [22,23]. Generally, the abovementioned compounds can be indexed to the Li_2O-WO_3-MgO ternary phase diagram, as plotted in Fig.1, wherein the $Li_2W_2O_7$ [24] and $MgWO_4$ [25] compounds with good microwave dielectric properties were also added.

There is a largely unexploited area in the Li_2O-rich part of the ternary phase diagram (Fig.1). We have noticed that while Li_4MgWO_6, a single monoclinic rock salt structure when calcined at 600 °C, was first synthesized by Mandal et al. as a precursor to prepare Sr_2MgWO_6 ceramics [26], no further work has been conducted on the functional properties of Li_4MgWO_6 to date. In this work, Li_4MgWO_6 ceramic was synthesized, and its crystal structure, sintering behavior, and microwave dielectric properties were studied.

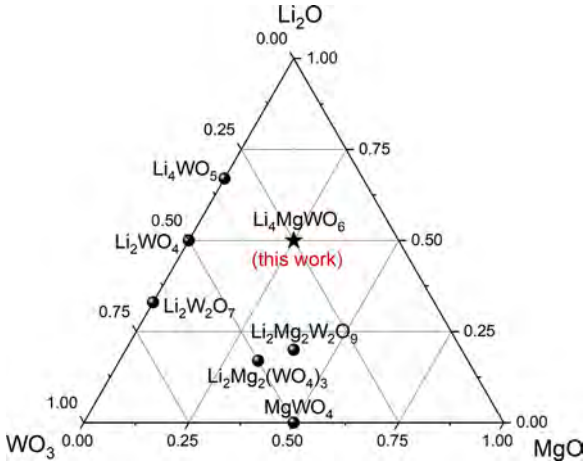

Fig. 1. Phase diagrams of the Li_2O-WO_3-MgO ternary system.

2. Materials and methods

Ceramic Li_4MgWO_6 was synthesized by the conventional solid-state reaction method. All the reactants, the $Mg(OH)_2{\bullet}4MgCO_3{\bullet}5H_2O$ (99.00 %), Li_2CO_3 (99.90 %), and WO_3 (99.90 %), were mixed by ball milling for 8 h in a nylon jar using zirconia balls and ethyl alcohol as the media. The slurries were dried for 6 h and then calcined at 750 °C for 4 h. The powders were then reground using the same method as above for 3 h. After drying, the resulting powders were granulated by adding an 8% polyvinyl alcohol (PVA) in an agate mortar. They were shaped into cylinders of diameter 12 mm and length 6 mm under a pressure of 22 MPa. Tungsten trioxide has a sublimation temperature of about 900 °C [27]. To prevent the WO_3 from subliming at the sintering temperature range, we put the samples on an Al_2O_3 groove with an Al_2O_3 crucible covered, and the interface between the crucible and the groove was buried with sufficient WO_3 powder, in which the sacrificial WO_3 powder provided a WO_3-rich atmosphere during the sintering. Then a giant Al2O3 crucible covered this whole set to preserve the WO_3-rich atmosphere. In this way, the samples were sintered in a controlled WO_3-rich atmosphere from 910 °C to 990 °C for 4 h.

The bulk densities were measured by the Archimedes' method, and the relative densities were calculated as the ratios of the observed densities to the theoretical densities. The X-ray powder diffraction patterns were scanned in 2θ ranges from 13° to 90° with a step size of 0.0131°, measured on a laboratory X-ray diffractometer (Philips X'Pert Pro MPD, Netherlands). The Rietveld method was conducted using the General Structure Analysis System (GSAS) coupled with the EXPGUI program to perform structure refinement [28,29]. The TG-DSC (thermogravimetric-differential scanning calorimeter) signals were obtained using a simultaneous thermal analysis (Netzsch STA 449C, Germany) with a heating rate of 10 °C/min in dry air. The shrinkage curves of the samples were measured on a horizontal loading dilatometer (Netzsch, Germany). The polished and thermally etched surface morphologies were observed by scanning electron microscopy (SEM, FEI Inspect F, England). Before SEM observations, the ceramic samples were polished on abrasive paper (1200 mesh) and thermally etched at temperatures of 30 °C below the sintering temperatures for 30 min. High-resolution transmission electron microscopy (HR-TEM) images and selected area electron diffractions (SAEDs) were obtained on a TEM microscope (Tecnai G2 F20 S-Twin TMP, USA) operated at 200 kV. Microwave dielectric properties were measured by a network analyzer (Agilent Technologies E5071C, USA) using the Hakki–Coleman method in TE011 mode [30]. The temperature coefficients of the resonant frequency (τ_f) were measured by the network analyzer coupled with a temperature chamber (DELTA 9023, Delta Design, USA), and calculated using the relation:

$$\tau_f = \frac{f_2 - f_1}{f_1(t_2 - t_1)} \quad (1)$$

where f_1 and f_2 represent the resonant frequencies at t_1 = 25 °C and t_2 = 85 °C, respectively. Dielectric permittivity variation in the temperature range of -55 to 125 °C was measured under 1 MHz frequency by a precision LCR meter (Agilent 4284A, USA) and an automatic temperature controller. The temperature coefficient of permittivity (τ_ε) was obtained by:

$$\tau_\varepsilon = \frac{\varepsilon_2 - \varepsilon_1}{\varepsilon_1(t_2' - t_1')} \quad (2)$$

where ε_1 is the permittivity at $t_1' = 25$ °C and ε_2 is the permittivity within 25 °C $< t_2' \leq$ 125 °C. The thermal expansion coefficient (α_L) was measured by a thermo-mechanical analysis (TMA, Netzsch DIL 420C, Germany).

3. Results and discussions

Fig.2 shows the XRD patterns of the Li_4MgWO_6 ceramics sintered at temperatures ranging from 910 to 990 °C for 4 h. The patterns can be indexed to the orthorhombic structure according to the profile of the $Li_3Mg_2NbO_6$ (JCPDS no. 86-0346) phase with the space group *Fddd* (70). Impure peaks, at around 2θ = 18.8 ° and 21.0 °, with low intensities indicated a tiny amount secondary phase was formed in the samples sintered above 900 °C. Based on the XRD data of the raw powders (Fig. S1), there is a monoclinic–orthorhombic phase transition driven by the temperature change from 800 °C to 900 °C. According to the peak profile of the monoclinic phase, the secondary phase might be the unreacted monoclinic Li_4MgWO_6 phase, which can be indexed according to the model of Li_5ReO_6 (JCPDS no. 82-0929) in the C2/m (12) space group. However, the Rietveld refinement results indicated that the weight fractions of the monoclinic secondary phase were relatively small (*wt.*% = 1–2 %) when the sintering temperature exceeded 930 °C, as shown in Fig.2 (c). Hence, the effects of the monoclinic phase on the structural and dielectric properties can be negligible. For more information on the reactions of the raw powders, see Eqs. S1–S8. Similarly, a cubic-orthorhombic phase transition has been reported for Li_4WO_5 ceramic in the temperature range from 680 °C to 750 °C [20]. These temperature-driven phase transitions for tungstate may be ascribed to the structure variation of tungsten trioxide with the temperature change. WO_3 is tetragonal at temperatures above 740 °C and is orthorhombic from 330 to 740 °C [31].

The Rietveld refinement profile of the Li_4MgWO_6 ceramic sintered at 950 °C is shown in Fig.3 (a), and the insert image exhibits the schematic of the crystal structure for the orthorhombic phase. The orthorhombic Li_4MgWO_6 phase has a crystal symmetry in an ordered rock-salt type, namely the *Fddd* space group. In this structure, the cations and anions are octahedrally coordinated by each other, similar to that of the $Li_3Mg_2NbO_6$ prototype [32]. The SAED pattern (Fig.3 (b)) for the orthorhombic Li_4MgWO_6 ceramic exhibits superlattice reflections arising from the cation ordering, which may be ascribed to the Li/Mg ordered arrangement over a superstructure period. The HR-TEM image (Fig.3 (c)) confirmed the ordered and layered structure for the orthorhombic Li_4MgWO_6 phase. The corresponding structural characteristics for the monoclinic Li_4MgWO_6 ceramic calcined at 750 °C are shown in Fig. S2. The monoclinic phase has a rock-salt superstructure as well but a different site symmetry (*C2/m*). The detailed crystallographic data derived from the refinement results for both structures are shown in Table S1.

Fig.4 shows the TG-DSC results for the Li_4MgWO_6 raw powder and linear shrinkage curve of the Li_4MgWO_6 ceramic as a function of temperature. The mass loss stages at temperatures below 700 °C were attributed to the decomposition of raw powder (dehydration and carbonate decomposition), and the slight mass loss at temperatures above 709 °C may be ascribed to the WO_3 sublimation in air [27]. According to the phase types of raw powders in the wide temperature range (Fig. S1), the endothermic peak located at 626 °C was related to the generation of the monoclinic phase, and two of the intense peaks ranging from 700 to 800 °C corresponded to the phase transition process from the monoclinic to the orthorhombic and the formation of the orthorhombic Li_4MgWO_6 phase, respectively. The shrinkage curve indicated that the densification process started at around 820 °C, the temperature near the formation period of the orthorhombic Li_4MgWO_6 phase, and the fastest contraction rate was at about 925 °C.

SEM images of the polished and thermally etched surfaces of the Li_4MgWO_6 samples sintered at the temperature range from 910 to 990 °C for 4 h were shown in Fig.5 (a–e), and the insert graphs show the grain size distributions and the average grain sizes. The grains were small, and numerous micropores were observed in the sample sintered at 910 °C, which indicated insufficient sintering. Neat and uniform grains were observed for the samples sintered at 930 °C and 950 °C, and no apparent micropores were detected in these well-sintered samples. The grain boundaries appeared to melt in the sample sintered at 970 °C. As the sintering temperature increased further to 990 °C, the grain boundaries of the sample melted more severely, and pores became larger, indicated oversintering. The average grain size increased continuously with the rising temperature. The morphologies of the cross-sections and surfaces of the as-sintered samples are shown in Fig. S3 and Fig. S4, respectively. Both the surface and cross-section morphologies showed that the sample sintered at 950 °C had the most highly densified microstructures. Compared Fig. 5 with Fig. S4, it can be seen the pores were further eliminated after the polishing and thermally etching.

The relative density (ρ_{re}) of the Li_4MgWO_6 ceramics as a function of the sintering temperature is shown in Fig.6 (a). With the increasing temperature, the ρ_{re} first increased, peaked at 95.66 % (theoretical density was 5.08 g/cm^3) at 950 °C and then decreased. The porosity ($P = 1\text{-}\rho_{re}$) variation followed the changing trend of the number of pores in the microstructures, as indicated in Fig. 5. The optimum relative density of the samples was higher than that of a few typical Li-containing

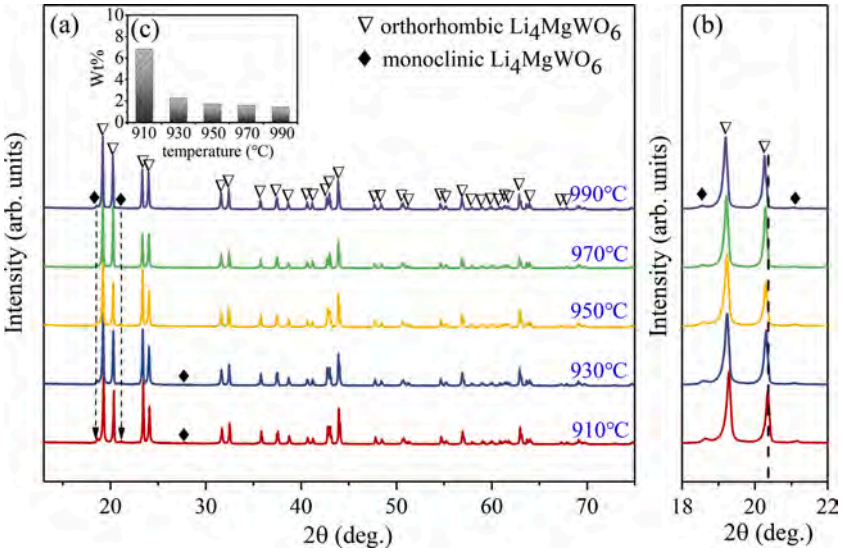

Fig. 2. (a) XRD patterns of the Li_4MgWO_6 ceramics sintered at 910 – 990 °C for 4 h. (b) Enlarged image of the XRD patterns ranges from 18 to 22 degrees. (c) Weight fractions (*wt.*%) of the monoclinic secondary phase.

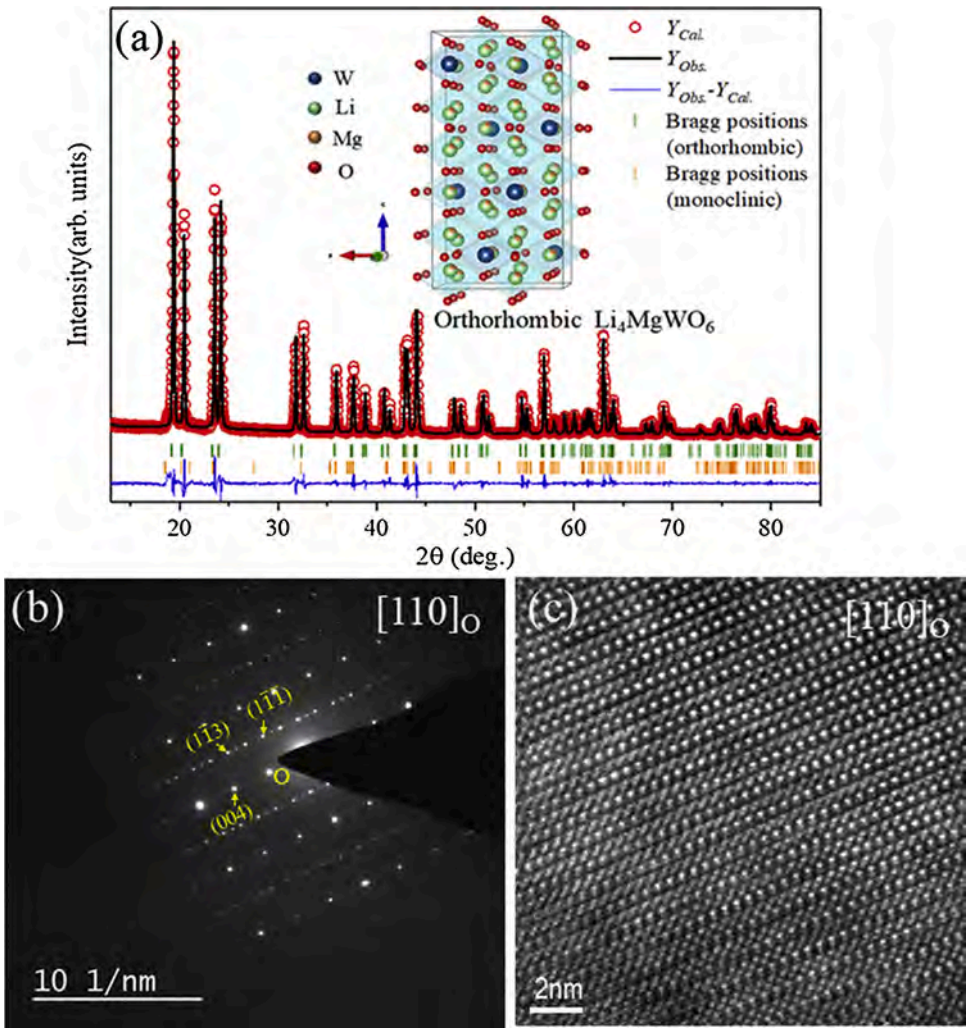

Fig. 3. (a) Rietveld refinement profile of Li_4MgWO_6 ceramic sinter at 950 °C for 4 h, the insert image was the schematic of the orthorhombic crystal structure for Li_4MgWO_6. (b) SAED pattern of the orthorhombic Li_4MgWO_6 taken along [110] zone axis and (c) the corresponding HR-TEM image.

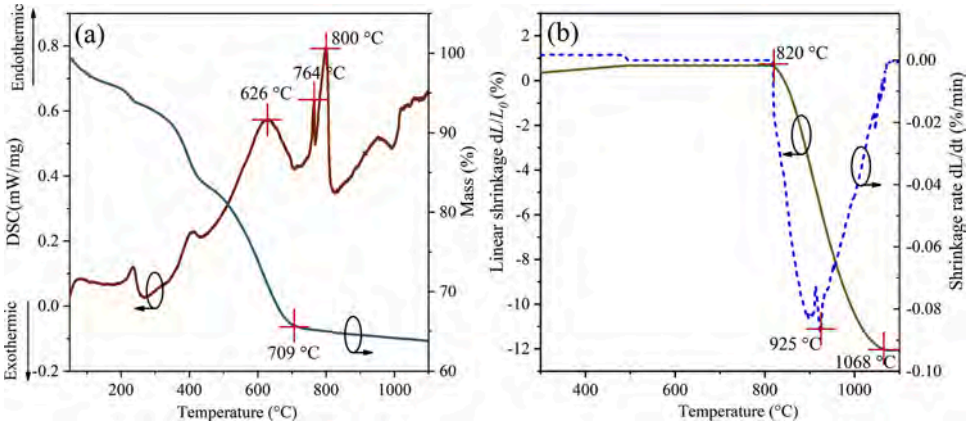

Fig. 4. (a) TG-DSC of the Li_4MgWO_6 raw powder and (b) linear shrinkage and shrinkage rate curves of the Li_4MgWO_6 ceramic.

ceramics sintered at relatively higher temperatures, such as Li_2TiO_3 (ρ_{re} ~93 %, 1300 °C) [33], $Li_2Mg_3TiO_6$ (ρ_{re} ~94 %, 1360 °C) [34], and Li_2MgTiO_4 (ρ_{re} ~91 %, 1360 °C) [35]. These ceramics showed highly porous microstructures because of the lithia evaporation at above 1000 °C [36]. It is reasonable that, to some extent, the high density was attained because the Li_4MgWO_6 sample can be densified below the evaporating point of lithium oxide. Similar degrees of high densifications were also achieved in two other lithium magnesium tungstate ceramics of $Li_2Mg_2W_2O$ (ρ_{re} ~95 %, 920 °C) [22] and $Li_2Mg_2(WO_4)_3$ (ρ_{re} ~96 %, 800 °C) [23] that were sintered below 1000 °C.

The relative permittivity (ε_r) showed a similar variation to the relative density with the increasing temperature, as plotted in Fig.6 (b). The

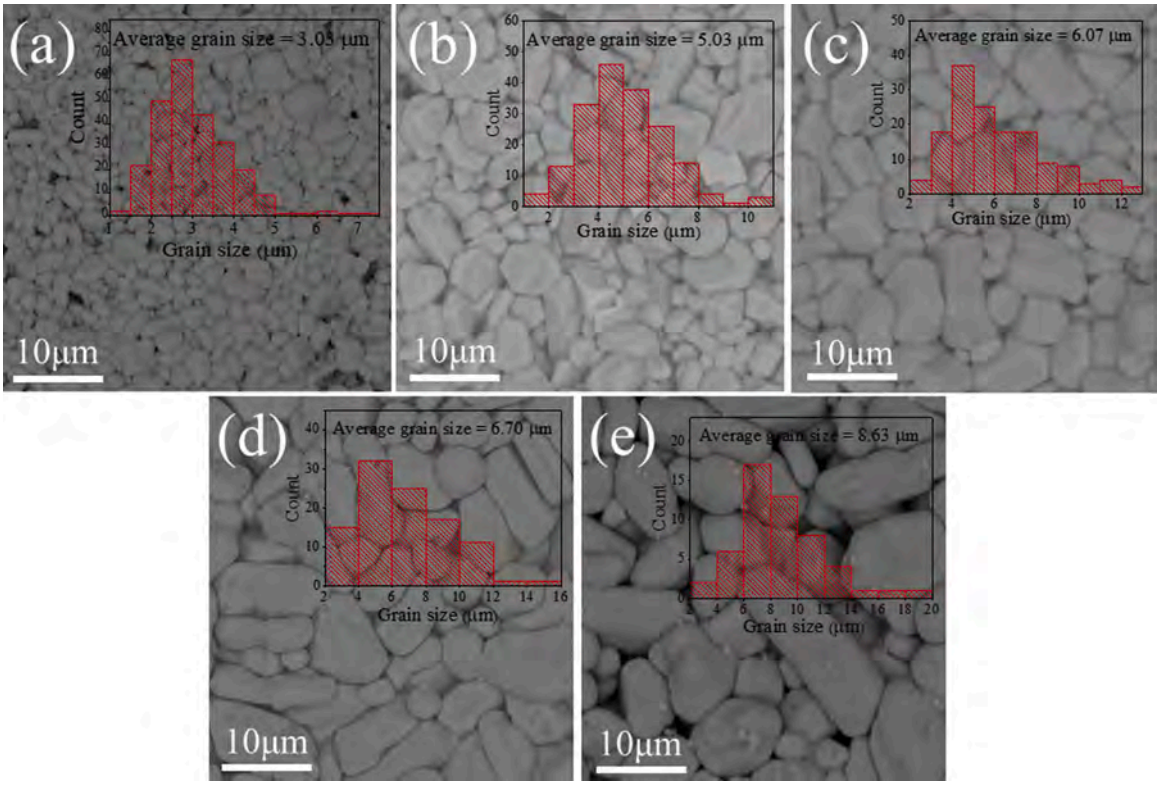

Fig. 5. SEM micrographs of the polished and thermally etched surface of the Li_4MgWO_6 ceramics sintered at (a) 910 °C, (b) 930 °C, (c) 950 °C, (d) 970 °C, and (e) 990 °C for 4 h. The insert graphs show the grain size distributions and the average grain sizes.

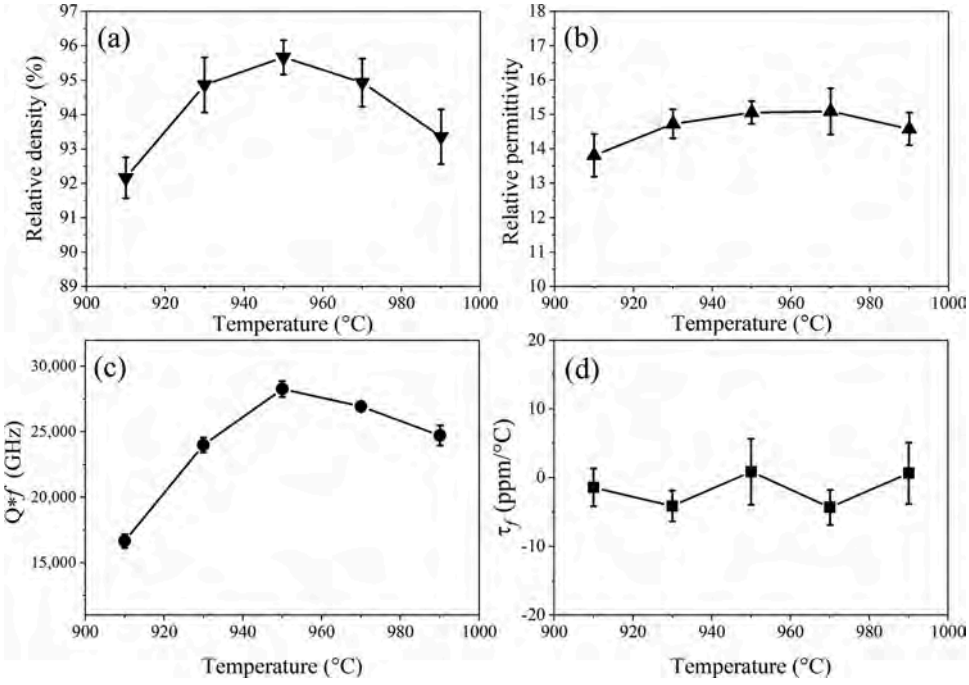

Fig. 6. (a) Relative density (ρ_{re}), (b) relative permittivity (ε_r), (c) Q × f value, and (d) temperature coefficient of the resonant frequency (τ_f) of the Li_4MgWO_6 ceramics as a function of temperature.

low relative permittivity of Li_4MgWO_6 can be attributed to the low ion dielectric polarizabilities of Li^+ (α = 1.20 Å^3) and Mg^{2+} (α = 1.32 Å^3) and moderate ionic polarizability of W^{6+} (α = 3.20 Å^3) ions [37]. The magnitude of the theoretical relative permittivity contributed by the ionic polarizabilities for a known structure can be estimated by the Clausius-Mosotti equation [37]:

$$\varepsilon_{r(theo)} = \frac{3V_m + 8\pi\alpha_D}{3V_m - 4\pi\alpha_D} \quad (3)$$

where V_m is the volume of the unit cell, and α_D is the total molecular

polarizability. The α_D of Li_4MgWO_6 can be calculated by the following relationship:

$$\alpha_D(Li_4MgWO_6) = 4\alpha(Li^+) + \alpha(Mg^{2+}) + \alpha(W^{6+}) + 6\alpha(O^{2-}) \quad (4)$$

The $\varepsilon_{r(theo)}$ was calculated as 15.22 for the sample sintered at 950 °C, close to the observed ε_r value of 15.06, indicating that there were not many "rattling" or "compressed" cations and dipolar impurities that could lead to permittivity deviation in the Li_4MgWO_6 ceramic [37].

The Q×*f* values highly depend on porosity, and the variation of the Q×*f* values corresponded closely to the changing trend of the relative density, as shown in Fig. 6(c). However, for well-dense structures (ρ_{re} >95 %), the packing fraction plays a more crucial role in the dielectric loss [38]. The packing fraction (P.F) was defined as [38]:

$$Packing\ fraction = \frac{volume\ of\ the\ atoms\ in\ the\ cell}{volume\ of\ the\ unit\ cell} \times Z \quad (5)$$

where *Z* is 8 for the Li_4MgWO_6 ceramic. The packing fraction of the Li_4MgWO_6 ceramic sintered at 950 °C was calculated as 72.7 %, which was similar to the typical ceramics with the close packing rock-salt structures, such as $Li_3Mg_2NbO_6$ (P.F ~ 70.0 %) [39], Li_2MgTiO_4 (P.F ~ 75.1 %) [40], and Li_2TiO_3 (P.F ~ 73.0 %) [41]. Because of the highly packed crystal structures, all these ceramics showed relatively low dielectric losses.

The temperature coefficients of the resonant frequency (τ_f) are displayed in Fig.6 (d). In the sintering temperature range, the measured τ_f values are within the scope from -6.0 to +4.3 ppm/°C. The τ_f value has a relation with the temperature coefficient of the relative permittivity (τ_ε) as follows [42]:

$$\tau_f = -(\alpha_L + \frac{\tau_\varepsilon}{2}) \quad (6)$$

where α_L is the thermal expansion coefficient. Fig.7 (a) shows the relative permittivity as a function of temperature (-55 – 125 °C) at 1 MHz frequency. The insert image of Fig.7 (a) shows the τ_ε values in a wide temperature range ($t_2^{'}$ = 30–125 °C, $t_1^{'}$ = 25 °C), and the τ_ε value between 25 °C and 85 °C was -10.1 ppm/°C. The sample has a linear thermal expansion, and α_L has a relatively large value of +13.2 ppm/°C between 25 °C and 85 °C, as shown in Fig. 7 (b). Thus, the τ_f value can be calculated by Eq. 6, the result value was -8.15 ppm/°C and not far from the measure ones (0.9 ± 3.4 ppm/°C). This deviation can be ascribed to the different measured frequencies, and a similar phenomenon was reported in other literature [43]. According to Bosman and Havinga's expression, three effects contribute to the temperature dependence of relative permittivity [44]. The former two effects (A and B) are associated with the volume-dependent contribution, and the sum of A and B generally has a small value for oxides, equal to about 6~7 ppm/°C for materials with a permittivity of 15 [44]. The third effect (C) plays a more significant role in τ_ε, related to the temperature dependence of the macroscopic polarizability at constant volume. The macro thermal expansion of ceramic samples is closely correlated to the asymmetric anharmonic vibrations of chemical bonds, directly affected by the binding energy and bond length [45]. Therefore, the near-zero τ_f values herein can be ascribed to the small dependence of the polarizability on temperature, moderate asymmetric anharmonic vibrations of chemical bonds, and the opposite signs between α_L and τ_ε in the temperature range from 25 °C to 85 °C.

Table 1 compares the microwave dielectric properties among some typical compounds with intrinsically low sintering temperatures and low permittivities. As we have mentioned in section 1, near-zero τ_f values are scarce among the low-permittivity compounds. Due to its novel temperature stability and relatively low dielectric loss, Li_4MgWO_6 shows advantages over the reported dielectrics. To verify the compatibility of the ceramic with Ag electrode, the Li_4MgWO_6 green body with Ag coatings was co-fired at 950 °C for 4 h. Fig. S5 shows the cross-section SEM image and EDS line scan of the Li_4MgWO_6 ceramic co-fired with Ag electrode. No obvious chemical reaction between the electrode and ceramic matrix was observed, and the EDS line scan spectrum indicated

Table 1
Sintering temperature and microwave dielectric properties of some typical compounds with low ε_r and low densification temperature.

composition	S.T. (°C)	ε_r	Q×*f* (GHz)	τ_f (ppm/°C)	Ref.
$LiWVO_6$	700	11.5	13,300	+163.8	[19]
$LiMoVO_6$	640	13.3	12,500	+101.0	[19]
Li_2MoO_4	540	5.5	46,000	−160.0	[18]
Li_2WO_4	650	5.5	62,000	−146.0	[21]
$Li_2Mg_2W_2O_9$	920	11.5	31,900	−66.0	[22]
$Li_2Mg_2(WO_4)_3$	800	8.2	90,000	−52.4	[23]
$Bi_2Mo_3O_{12}$	610	19.0	21,800	−215.0	[46]
BaV_2O_6	550	11.2	42,800	+28.2	[47]
$ZnMoO_4$	850	8.1	48,300	−121.8	[48]
$Li_6B_4O_9$	640	5.95	41,800	−72.0	[49]
$Ba_2NdV_3O_{11}$	880	12.05	23,000	−7.7	[50]
$Ba_2SmV_3O_{11}$	880	12.19	27,100	−16.2	[50]
Li_4WO_5	890	8.6	23,100	−2.6	[20]
Li_4MgWO_6	950	15.06 ± 0.33	28,300 ± 600	0.9 ± 3.4	This work

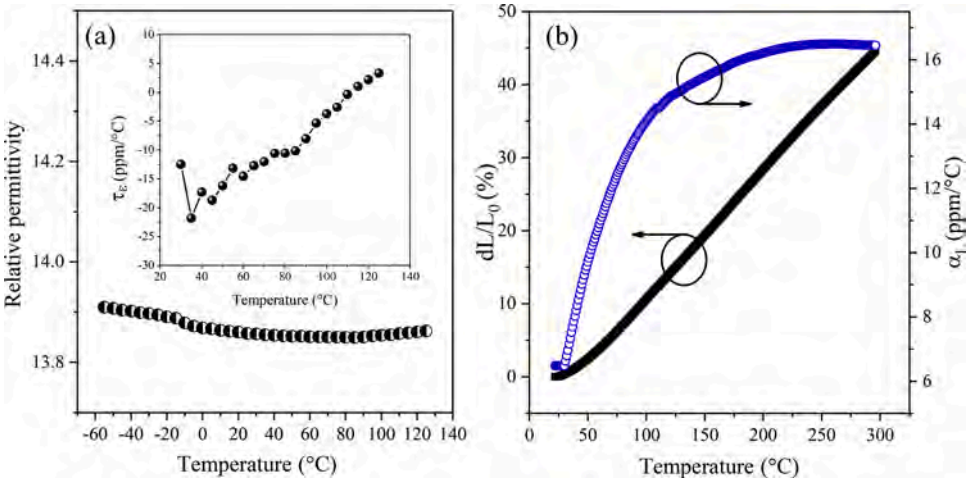

Fig. 7. (a) Relative permittivities of the Li_4MgWO_6 ceramic sintered at 950 °C for 4 h as a function of temperature (-55 – 125 °C) measured at 1 MHz, the insert image shows the τ_ε values in a wide temperature range ($t_2^{'}$ = 30 – 125 °C, $t_1^{'}$ = 25 °C). (b) Thermal expansion (dL/L_0) and the thermal expansion coefficient (α_L) for the Li_4MgWO_6 ceramic sintered at 950 °C for 4 h.

almost no Ag diffusion into the ceramic matrix. With the above advantages, Li_4MgWO_6 is a promising low-permittivity candidate material for LTCC applications.

4. Conclusions

In this contribution, a novel Li_4MgWO_6 ceramic was synthesized via the conventional solid-state reaction method, and the structural characteristics, sintering behavior, and microwave dielectric properties were studied for the first time. The XRD patterns of the samples taken over a wide temperature range (400 –1000 °C) revealed a monoclinic-orthorhombic phase transition for the Li_4MgWO_6 ceramic ranging from 800 °C to 900 °C. A tiny amount (wt.% = 1–2 %) of the untransformed monoclinic secondary phase was retained in the orthorhombic main phase for the ceramics sintered above 930 °C. The SAED and HR-TEM photographs taken along the low-index zone axis confirmed the ordered and layered rock-salt superstructures for the orthorhombic Li_4MgWO_6 samples. The shrinkage curve showed that the densification of the specimen proceeded in a wide temperature range from 820 °C to 1068 °C, and the SEM photographs and relative density curves indicated the sample had the highest densification at 950 °C. Samples were sintered in a WO_3-rich atmosphere provided by a designed device to prevent WO_3 from subliming at the sintering range. The sample sintered at 950 °C for 4 h showed a high relative density of 95.66 % and a high packing fraction of 72.7 %. The optimum microwave dielectric properties were obtained with $\varepsilon_r = 15.06 \pm 0.33$, $Q \times f = 28{,}300 \pm 600$ GHz (f = 10.1 GHz), and $\tau_f = 0.9 \pm 3.4$ ppm/°C. Due to its intrinsic low sintering temperature, novel temperature stability, relatively low dielectric loss, and good chemical compatibility with Ag electrodes, Li_4MgWO_6 is a promising material for LTCC applications.

Declaration of Competing Interest

The authors declare that they have no known competing financial interests or personal relationships that could have appeared to influence the work reported in this paper.

Acknowledgments

This work was supported by the National Natural Science Foundation of China (Grant No. 52102123 and 62171080).

Appendix A. Supplementary data

Supplementary material related to this article can be found, in the online version, at doi:https://doi.org/10.1016/j.jeurceramsoc.2021.09.010.

References

[1] M.T. Sebastian, R. Ubic, H. Jantunen, Microwave Materials and Applications, John Wiley & Sons, 2017.
[2] Y. Guo, H. Ohsato, K.-i. Kakimoto, Characterization and dielectric behavior of willemite and TiO2-doped willemite ceramics at millimeter-wave frequency, J. Eur. Ceram. Soc. 26 (10) (2006) 1827–1830.
[3] X. Zhang, Z. Fang, H. Yang, P. Zhao, X. Zhang, Y. Li, Z. Xiong, H. Yang, S. Zhang, B. Tang, Lattice evolution, ordering transformation and microwave dielectric properties of rock-salt $Li_{3+x}Mg_{2-2x}Nb_{1-x}Ti_{2x}O_6$ solid-solution system: a newly developed pseudo ternary phase diagram, Acta Mater. 206 (2021), 116636.
[4] Z. Xiong, B. Tang, X. Zhang, C. Yang, Z. Fang, S. Zhang, Low-fire processing and microwave dielectric properties of LB glass-doped $Ba_{3.75}Nd_{9.5}Ti_{17.5}(Cr_{0.5}Nb_{0.5})_{0.5}O_{54}$ ceramic, J. Am. Ceram. Soc. (2020) n/a(n/a).
[5] H. Ohasto, T. Tsunooka, M. Ando, Y. Ohishi, Y. Miyauchi, Millimeter-wave dielectric ceramics of alumina and forsterite with high quality factor and low dielectric constant, J. Korean Ceram. Soc. 40 (4) (2003) 350–353.
[6] K.P. Surendran, N. Santha, P. Mohanan, M.T. Sebastian, Temperature stable low loss ceramic dielectrics in (1-x)$ZnAl_2O_4$-xTiO_2 system for microwave substrate applications, Eur. Phys. J. B 41 (3) (2004) 301–306.
[7] H. Ohsato, M. Terada, K. Kawamura, Fabrication conditions of diopside for millimeterwave dielectrics, J. Appl. Phys. 51 (2012), 09LF02.
[8] L.L. Yuan, J.J. Bian, Microwave dielectric properties of the lithium containing compounds with rock salt structure, Ferroelectrics 387 (1) (2009) 123–129.
[9] L.-X. Pang, D. Zhou, Microwave dielectric properties of low-firing Li_2MO_3 (M=Ti, Zr, Sn) ceramics with B_2O_3–CuO addition, J. Am. Ceram. Soc. 93 (11) (2010) 3614–3617.
[10] H.-H. Guo, D. Zhou, C. Du, P.-J. Wang, W.-F. Liu, L.-X. Pang, Q.-P. Wang, J.-Z. Su, C. Singh, S. Trukhanov, Temperature stable $Li_2Ti_{0.75}(Mg_{1/3}Nb_{2/3})_{0.25}O_3$-based microwave dielectric ceramics with low sintering temperature and ultra-low dielectric loss for dielectric resonator antenna applications, J. Mater. Chem. C 8 (14) (2020) 4690–4700.
[11] J.J. Bian, J.Y. Wu, L. Wang, Structural evolution, sintering behavior and microwave dielectric properties of (1−x)Li_3NbO_4–xLiF (0≤x≤0.9), J. Eur. Ceram. Soc. 32 (6) (2012) 1251–1259.
[12] P. Zhang, H. Xie, Y. Zhao, X. Zhao, M. Xiao, Low temperature sintering and microwave dielectric properties of $Li_3Mg_2NbO_6$ ceramics doped with Li_2O–B_2O_3–SiO_2 glass, J. Alloys. Compd. 690 (2017) 688–691.
[13] M.T. Sebastian, Dielectric Materials for Wireless Communication, Elsevier, 2010.
[14] R.C. Pullar, C. Lai, F. Azough, R. Freer, N.M. Alford, Novel microwave dielectric LTCCs based upon V_2O_5 doped $M^{2+}Cu_2Nb_2O_8$ compounds (M_{2+}=Zn, Co, Ni, Mg and Ca), J. Eur. Ceram. Soc. 26 (10) (2006) 1943–1946.
[15] D.-W. Kim, D.-K. Kwon, S.H. Yoon, K.S. Hong, Microwave dielectric properties of rare-earth ortho-niobates with ferroelasticity, J. Am. Ceram. Soc. 89 (12) (2006) 3861–3864.
[16] M.T. Sebastian, H. Jantunen, Low loss dielectric materials for LTCC applications: a review, Int. Mater. Rev. 53 (2) (2008) 57–90.
[17] H.-H. Guo, D. Zhou, L.-X. Pang, Z.-M. Qi, Microwave dielectric properties of low firing temperature stable scheelite structured (Ca,Bi)$(Mo,V)O_4$ solid solution ceramics for LTCC applications, J. Eur. Ceram. Soc. 39 (7) (2019) 2365–2373.
[18] D. Zhou, C.A. Randall, H. Wang, L.-X. Pang, X. Yao, Microwave dielectric ceramics in Li_2O–Bi_2O_3–MoO_3 system with ultra-low sintering temperatures, J. Am. Ceram. Soc. 93 (4) (2010) 1096–1100.
[19] H. Xiang, C. Li, Y. Tang, L. Fang, Two novel ultralow temperature firing microwave dielectric ceramics $LiMVO_6$ (M=Mo, W) and their chemical compatibility with metal electrodes, J. Eur. Ceram. Soc. 37 (13) (2017) 3959–3963.
[20] J. Li, L. Fang, H. Luo, J. Khaliq, Y. Tang, C. Li, Li_4WO_5: a temperature stable low-firing microwave dielectric ceramic with rock salt structure, J. Eur. Ceram. Soc. 36 (1) (2016) 243–246.
[21] D. Zhou, C.A. Randall, L.-X. Pang, H. Wang, J. Guo, G.-Q. Zhang, X.-G. Wu, L. Shui, X. Yao, Microwave dielectric properties of Li2WO_4 ceramic with ultra-low sintering temperature, J. Am. Ceram. Soc. 94 (2) (2011) 348–350.
[22] H. Guo, L. Fang, X. Jiang, J. Li, F. Lu, C. Li, A novel low-firing and low loss microwave dielectric ceramic $Li_2Mg_2W_2O_9$ with corundum structure, J. Am. Ceram. Soc. 98 (12) (2015) 3863–3868.
[23] J. Zhang, R. Zuo, Synthesis and microwave dielectric properties of $Li_2Mg_2(WO_4)_3$ ceramics, Mater. Lett. 158 (2015) 92–94.
[24] J. Chen, C. Li, D. Wang, H. Xiang, L. Fang, Preparation, crystal structure, and dielectric characterization of $Li_2W_2O_7$ ceramic at RF and microwave frequency range, J. Adv. Dielectr. 07 (01) (2017), 1720001.
[25] R.C. Pullar, S. Farrah, N.M. Alford, $MgWO_4$, $ZnWO_4$, $NiWO_4$ and $CoWO_4$ microwave dielectric ceramics, J. Eur. Ceram. Soc. 27 (2) (2007) 1059–1063.
[26] T.K. Mandal, J. Gopalakrishnan, New route to ordered double perovskites: synthesis of rock salt oxides, Li4MWO6, and their transformation to Sr2MWO6 (M = Mg, Mn, Fe, Ni) via metathesis, Chem. Mater. 17 (9) (2005) 2310–2316.
[27] M. Valigi, S. De Rossi, D. Gazzoli, G. Minelli, A structural, thermogravimetric and magnetic study of the WO_x-TiO_2 system, J. Mater. Sci. 20 (1) (1985) 71–76.
[28] A. Larson, R. Von Dreele, GSAS General Structure Analysis System, Program and Handbook, Los Alamos National Laboratory Report LAUR 86-748, University of California, USA, 2000.
[29] B. Toby, EXPGUI, a graphical user interface for GSAS, J. Appl. Crystallogr. 34 (2) (2001) 210–213.
[30] B.W. Hakki, P.D. Coleman, A dielectric resonator method of measuring inductive capacities in the millimeter range, IRE Trans. Microw. Theory Tech. 8 (4) (1960) 402–410.
[31] E. Lassner, W.-D. Schubert, Tungsten: Properties, Chemistry, Technology of the Element, Alloys, and Chemical Compounds, Springer Science & Business Media, 2012.
[32] X. Zhang, B. Tang, Z. Fang, H. Yang, Z. Xiong, L. Xue, S. Zhang, Structural evolution and microwave dielectric properties of a novel $Li_3Mg_{2-x/3}Nb_{1-2x/3}Ti_xO_6$ system with a rock salt structure, Inorg. Chem. Front. 5 (12) (2018) 3113–3125.
[33] J.J. Bian, Y.F. Dong, New high Q microwave dielectric ceramics with rock salt structures: (1−x)Li2TiO_3+xMgO system (0≤x≤0.5), J. Eur. Ceram. Soc. 30 (2) (2010) 325–330.
[34] H. Wu, E.S. Kim, Correlations between crystal structure and dielectric properties of high-Q materials in rock-salt structure Li2O–MgO–BO2 (B = Ti, Sn, Zr) systems at microwave frequency, RSC Adv. 6 (53) (2016) 47443–47453.
[35] Y.-W. Tseng, J.-Y. Chen, Y.-C. Kuo, C.-L. Huang, Low-loss microwave dielectrics using rock salt oxide Li2MgTiO4, J. Alloys. Compd. 509 (33) (2011) L308–L310.
[36] Y. Iida, Evaporation of lithium oxide from solid solution of lithium oxide in nickel oxide, J. Am. Ceram. Soc. 43 (3) (1960) 171–172.
[37] R.D. Shannon, Dielectric polarizabilities of ions in oxides and fluorides, J. Appl. Phys. 73 (1) (1993) 348–366.
[38] S. Liu, B. Tang, M. Zhou, P. Zhao, Q. Xiang, X. Zhang, Z. Fang, S. Zhang, Microwave dielectric characteristics of high permittivity Ca0.35Li0.25Nd0.35Ti1-x(Zn1/3Ta2/3)xO3 ceramics (x = 0.00–0.12), Ceram. Int. 45 (7, Part A) (2019) 8600–8606.

[39] G. Wang, D. Zhang, X. Huang, Y. Rao, Y. Yang, G. Gan, Y. Lai, F. Xu, J. Li, Y. Liao, C. Liu, L. Jin, V.G. Harris, H. Zhang, Crystal structure and enhanced microwave dielectric properties of Ta5+ substituted Li3Mg2NbO6 ceramics, J. Am. Ceram. Soc. 103 (1) (2020) 214–223.
[40] P. Wang, Y.R. Wang, J.X. Bi, H.T. Wu, Effects of Zn2+ substitution on the crystal structure, Raman spectra, bond energy and microwave dielectric properties of Li2MgTiO4 ceramics, J. Alloys. Compd. 721 (2017) 143–148.
[41] J. Zhang, R. Zuo, Low-temperature fired thermal-stable Li2TiO3–NiO microwave dielectric ceramics, J. Mater. Sci. Mater. Electron. 27 (8) (2016) 7962–7968.
[42] H.-H. Guo, D. Zhou, W.-F. Liu, L.-X. Pang, D.-W. Wang, J.-Z. Su, Z.-M. Qi, Microwave dielectric properties of temperature-stable zircon-type (Bi, Ce)VO_4 solid solution ceramics, J. Am. Ceram. Soc. 103 (1) (2020) 423–431.
[43] K. Cheng, Y. Tang, H. Xiang, C. Li, L. Fang, Y. Sun, Two novel low permittivity microwave dielectric ceramics Li2TiMO5 (M = Ge, Si) with abnormally positive τf, J. Eur. Ceram. Soc. 39 (8) (2019) 2680–2684.
[44] A.J. Bosman, E.E. Havinga, Temperature dependence of dielectric constants of cubic ionic compounds, Phys. Rev. 129 (4) (1963) 1593–1600.
[45] Y. Zhou, G. Gan, Z. Ge, J. Feng, S. Peng, Investigation of thermophysical properties of ZrO2-Sm3TaO7 ceramics, J. Asian Ceram. Soc. 9 (2) (2021) 629–638.
[46] D. Zhou, H. Wang, L.-X. Pang, C.A. Randall, X. Yao, Bi_2O_3–MoO_3 binary system: an alternative ultralow sintering temperature microwave dielectric, J. Am. Ceram. Soc. 92 (10) (2009) 2242–2246.
[47] U.A. Neelakantan, S.E. Kalathil, R. Ratheesh, Structure and microwave dielectric properties of ultralow-temperature cofirable $BaV2O_6$ ceramics, Eur. J. Inorg. Chem. 2015 (2) (2015) 305–310.
[48] P. Yadav, E. Sinha, Structural, photophysical and microwave dielectric properties of α-$ZnMoO_4$ phosphor, J. Alloys. Compd. 795 (2019) 446–452.
[49] D. Zhou, L.-X. Pang, D.-W. Wang, Z.-M. Qi, I.M. Reaney, High quality factor, ultralow sintering temperature $Li6B_4O_9$ microwave dielectric ceramics with ultralow density for antenna substrates, ACS Sustain. Chem. Eng. 6 (8) (2018) 11138–11143.
[50] C. Li, H. Xiang, M. Xu, J. Khaliq, J. Chen, L. Fang, Low-firing and temperature stable microwave dielectric ceramics: $Ba2LnV_3O_{11}$ (Ln = Nd, Sm), J. Am. Ceram. Soc. 101 (2) (2018) 773–781.